INFRASTRUCTURE MONITORING USING THE INTERFEROMETRIC SYNTHETIC APERTURE RADAR (INSAR) TECHNIQUE

Q. Gao [1,*] , M. Crosetto [1], O. Monserrat [1], R. Palama [1], A. Barra [1]

[1] Geomatics Research Unit, Centre Tecnològic de Telecomunicacions de Catalunya (CTTC/CERCA), Spain - qi.gao@cttc.cat

Commission III, WG III/3

KEY WORDS: InSAR, Deformation, Infrastructure, Persistent Scatterer Interferometry Sentinel-1.

ABSTRACT:

This paper focuses on the application of spaceborne radar interferometry as a tool for assisting the monitoring different types of infrastructures, including railways and highways. The Persistent Scatterer Interferometry (PSI) technique, the most advanced class of differential interferometric Synthetic Aperture Radar techniques (DInSAR), is used to generate the deformation maps, including the time series and the displacement velocity for each measured persistent scatterers. The dataset considered in this work consists of 261 SAR IW-SLC images acquired by the Sentinel-1 A/B satellites, between January 2016 and September 2021, over the metropolitan area of Barcelona. The infrastructures, especially railways and highways, not only cross the cities, but also connect them crossing non-urban areas. One main technical issue of monitoring infrastructures is the low density of persistent scatterers (PS) in rural areas. To improve the density, the processing chain combines the interferograms selection based on the coherence threshold. Also, for a better point selection, the Equivalent Spatial Coherence (Omega Factor) is tested.

1. INTRODUCTION

1.1 Background

A good and "healthy" infrastructure network is of vital importance to our society. Power, gas, and water distribution networks (power lines, pipelines, hydraulic canals, etc.), transport networks (roads, railways, etc.) or information networks (optic fibre) are "physically" founded on the earth surface. Moreover, some of the afore mentioned infrastructures, like earth dams or road/railway embankments, can be considered as geo-structures themselves, as they are directly built using soil materials. Earth surface and infrastructures are affected by catastrophic natural disasters (like earthquakes, floods, etc.) or by slow threats related to physical deterioration (material decay, erosion, etc.). Traditional monitoring of infrastructure displacement is usually limited to very few measurement points. With the new remote technologies from satellites, such as the Differential Interferometric Synthetic Aperture Radar (DInSAR) technique, we can now monitor infrastructures covering wide areas, continuously over time, in a cost-effective way.

DInSAR is playing an increasingly important role in the field of surface deformation monitoring. With the launch of Sentinel-1 satellite, the technique was significant further improvement with the new C-band sensor on-board (Rucci et al., 2012). Sentinel-1 has improved the data acquisition and, has increased considerably the DInSAR and PSI deformation monitoring potential (Barra et al., 2017, Huang et al., 2017), which improves the long-term geohazard monitoring capability over regional areas (Tang et al., 2015).

1.2 State of Art

PSI represents an advanced class of the Differential Interferometric Synthetic Aperture Radar (DInSAR) techniques. DInSAR techniques exploit the information contained in the radar image phase of at least two complex SAR images acquired at different times over the same area, that are used to form interferometric pairs. The PSI techniques make use of large stacks of SAR images acquired over the same area and employ advanced estimation techniques to derive the deformation estimates (Ferretti et al., 2000, 2001; Crosetto et al., 2016). This allows us deriving a deformation monitoring of higher precision and reliability. The PSI processing chains, which are using wide-area coverage satellite images, allows us to get a global look of deformation over a wide area, while keeping the capability to measure individual features, like structures and buildings. Therefore, it is an efficient and powerful tool for infrastructures monitoring. The PSI technique is sensitive to small deformations, in the order of millimetres. This high displacement sensitivity is a key characteristic to achieve an early detection of deformation phenomena.

2. STUDY AREA AND DATASET

2.1 Study Area

As involved in the PROMETEO (Predictive Infrastructure Maintenance using Intelligent Remote Monitoring and Integrated Dynamic Modelling) project, the objective of this research is to perform a wide-area, intelligent early-detection of deformation phenomena that concern infrastructures. This fully exploits the potentiality of DInSAR to monitor several infrastructures at the same time. This research work in particular concerns the monitoring of the infrastructure of the Catalan Railways (Ferrocarrils de la Generalitat de Catalunya - FGC). The covered area is the metropolitan area of Barcelona, which includes 10 main railways lines with almost 200 km in length, see Figure 1.

As a coastal city, Barcelona is topographically limited by the hills of Collserola and the rivers Llobregat and Besos. These topographical constraints create urban congestion and high residential densities, subjecting it to severe traffic congestion. The public transport network, including railways, metros, and highways, is essential for residents who live in Barcelona and

---

* Corresponding author: Q. Gao, qi.gao@cttc.cat

the satellite cities around it. The "health" of these essential infrastructures needs to be monitored to supply a reliable transport system.
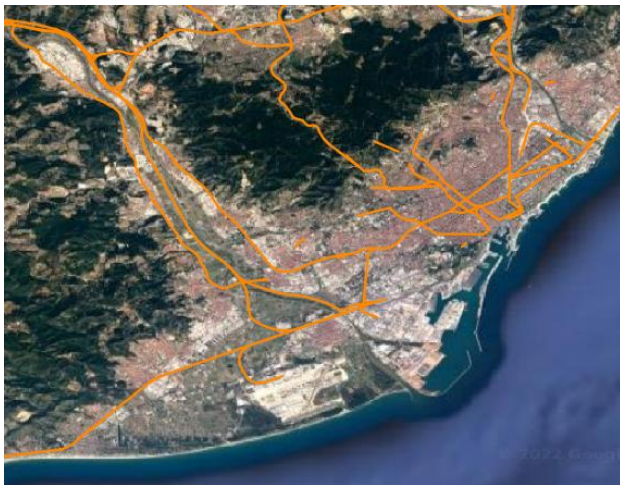

Figure 1. Study area and railway networks.

2.2 Dataset

The Sentinel-1 satellites are equipped with C-band Synthetic Aperture Radar (SAR) instruments, providing data in dual or single polarizations. Sentinel-1 provides data with a spatial resolution of approximately 4 by 14 m and a temporal resolution of 12 days (6 days considering the constellation A and B), in both VV and VH polarizations. In this study, complex signals recorded in the VV polarization were used to compute the deformations. One ground track (110) was considered, for which the incidence angle was approximately 39°. The Sentinel-1 satellite database corresponds to the period from January 2016 to September 2021. The SRTM Digital Elevation Model with 30-m resolution provided by NASA has been used to process the interferometric products.

Satellite	Sentinel-1
Sensor	A/B
Band	C
Wavelength	5.55 cm
Acquisition mode	Wide Swath
Polarization	VV
SAR product Complex	Single Look Complex
Acquisition orbit	Descending
Temporal period	24 January 2016–30 September 2021
Revisit period	6–12 days
Resolution	14 by 4 m
Incidence angle Track	39°
Number of SAR images	261

Table 1. Main acquisition parameters of the SAR satellite dataset

3. METHODOLOGY

3.1 PSI Chain

The processing chain for wide area deformation monitoring we use in this stud is the Persistent Scatterer Interferometry (PSI) implemented by CTTC, see the processing workflow in Figure 3. This monitoring can fully exploit the historical archives of InSAR data. The major challenge of this study is to tailor the processing parameters to maximise the measurement point

density over the infrastructures of interest and their neighbour areas. To achieve this, we are exploring different point selection methods with the combination of using a specific mask over the infrastructure.

In this study the PSI Chain mainly includes the following steps:

1) Pre-processing.
This step includes calibration of the images, image co-registration and interferograms generation.

2) Topographic error estimation.
In this step, the points are selected based on interferograms either the amplitude dispersion (DA) or the equivalent spatial coherence (Omega Factor). The selected points, which are the persistent scatterers (PS), are connected to form the interferogram network used for the topographic error estimation. A point with a low value of DA, which we consider is stable, is used as the reference point. The maximum temporal baseline of 30 days is specified for a better estimation of topographic error. From the original interferograms and the phase related to the topographic errors, we can generate the residuals, which will be used in the next step.
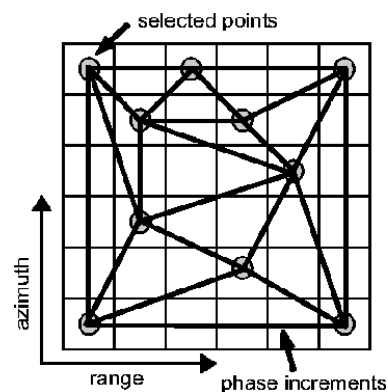

Figure 2. Points connection. The selected pixels are connected by edges (Mora, 2003).

3) Time series (TS) estimation
In this step, all the interferogram phases are set with respect to the same reference point. A pixel-wise processing is performed iteratively, which analyses over time the unwrapped interferometric phases. The Single Value Decomposition (SVD) least-squares method is used to compute the residuals and the outliers are excluded. The procedure is executed iteratively until there are no outliers, which is possible to correct the unwrapping errors. More details about phase unwrapping can be found in Biescas et al., 2007.
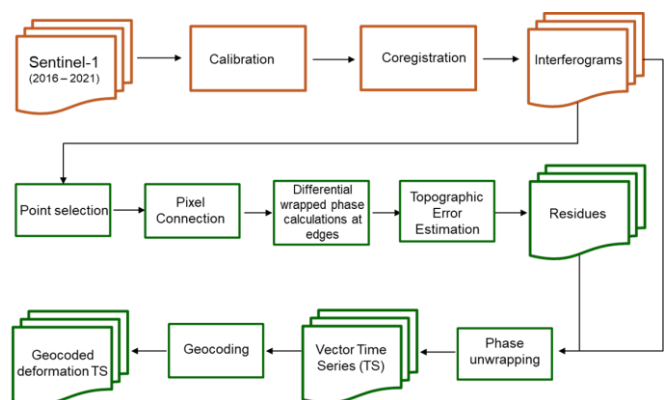

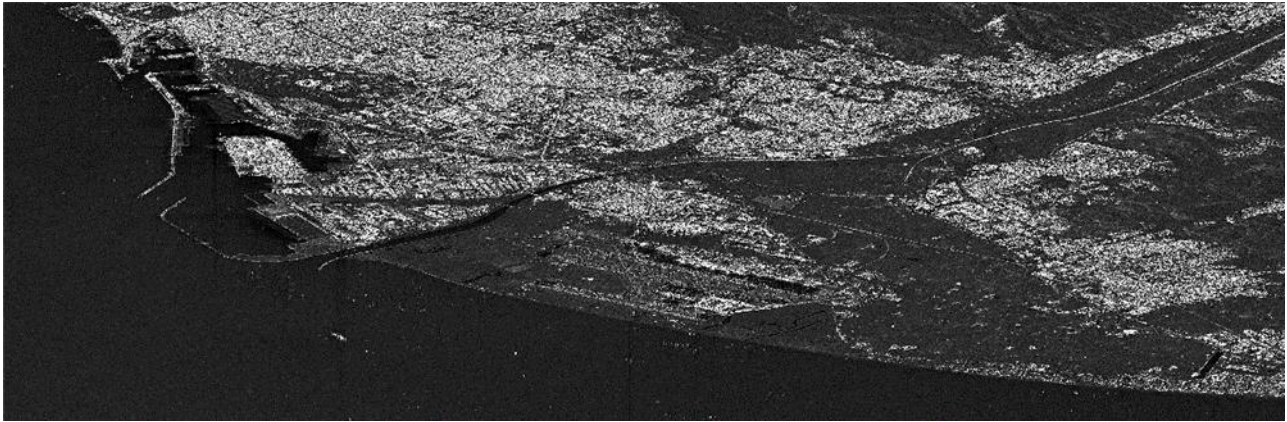**Figure 3**. Workflow of the procedure used in this work.

Figure 4. Omega factor over Barcelona (dark to bright indicates 0 to 1)

3.2 Interferograms Selection

One of the main challenging aspects of infrastructure monitoring is the density of points, especially outside of the cities, where PS are not dense enough. To improve this, we first performed the interferograms selection base on the coherence threshold to make sure the quality of the interferograms and in the meantime all of them are well connected. In this case, the coherence threshold is set at 0.36 and the minimum redundancy of the images is set at 6, see the network in Figure 5.
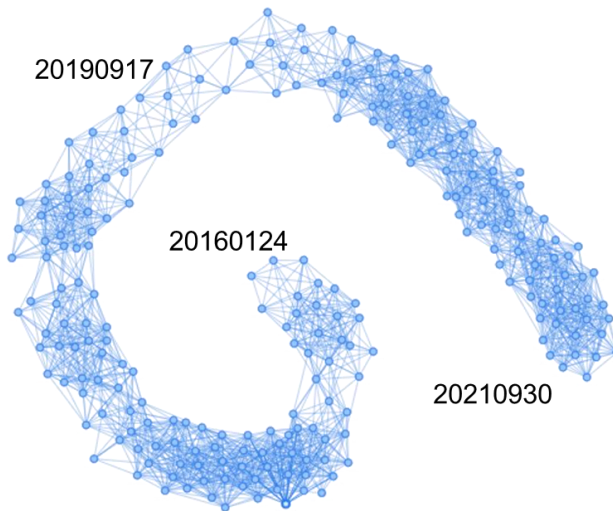

Figure 5. Image and interferogram network.

3.3 Omega factor

The omega factor, which is somehow equivalent to spatial coherence is used to select coherent points in the SAR interferograms. The method is included within the processing chain illustrated in (Pepe et al., 2015), which is the basis for the Small Baseline Subset (SBAS) interferometric processing chain. The implemented factor is given by:

$$\Omega(P) = \frac{1}{M}\left|\sum_{k=1}^{M} exp[j(\Delta\varphi(P) - \Delta\varphi_{LP}(P))]\right| \qquad (1)$$

where
P = the index which identifies a pixel
M = the number of interferograms
k = the interferogram index
$\Delta\varphi$ = the wrapped interferometric phase
$\Delta\varphi_{LP}$ = the low-pass estimate of the wrapped interferometric phase.

The calculation is performed on the wrapped interferograms. First, estimation of the spatial low-pass interferometric phase is computed using a boxcar averaging window, then the spatial low-pass phase is subtracted modulo-2π from the original interferometric phase, giving a high-pass estimate of the interferometric phase. For each pixel, the high-pass phasors are averaged coherently, to mitigate the effect of the phase noise. Then the module of the resultant vector is computed. The values of the extracted quantity are included between 0 and 1. The higher the value of omega the more coherent a pixel. In Figure 4, the omega map is shown over Barcelona.

4. RESULTS AND DISCUSSION

In this section, we describe several cases over the area of interest. The overall displacement velocity map of Figure 6 shows the stable status of points in most of the areas, and a good density is achieved in most parts of the infrastructures. However, we still found interesting places where points are not covered, an example is shown in Figure 7.

Figure 6. Displacement velocity map over railway network in Barcelona

The railway in Figure 7 crosses an area with agricultural fields, where we have little PS. Since the Sentinel-1 passes the study area in descending direction, the points over railways in north-south orientation have a higher density than

in east-west orientation. It could be explained that the density of the points is sensitive to the orientation of the railways. Looking into details of the velocity map, we found several regions where subsidence or uplift happen over the infrastructures. In the appended pages, a few examples are shown, which are (1) the subsidence over embankments of railway and highway, (2) the subsidence over the airport of Barcelona El-Prat, (3) examples of subsidence and uplift, (4) typical thermal dilation over the highway.

Figure 7. An example of the displacement velocity map where points have not covered the railways in an east-west direction.

(1) The subsidence over embankments of infrastructures is commonly seen in deformation studies due to the heavy transport. In both cases shown in Figure 8, the accumulated deformation is up to 30 mm over five years.

(2) The subsidence over the airport, which serves as a very important big infrastructure, cannot be neglected. The two areas show an accumulated subsidence of up to 40 mm. The main reason for these phenomena could be due to the intense underground water extraction activities.

(3) In this study, we observed several examples of deformation. Figure 10 shows one of these cases. PSI analysis indicates an accumulated subsidence up to 80 mm over the five years. In the meanwhile, continuous uplift up to 40mm occurs in the adjacent areas. Such movements could be interpreted as a result of the volume or structure changes in the soil, however, further studies need to be done to analyse these phenomena.

(4) In the last case, a typical thermal dilation with a seasonal cycle is presented over the highway. Thermal dilation is a typical component of deformation over bridges and viaducts (Qin et al., 2017).

5. CONCLUSIONS

In this study, the PSI chain of CTTC has been used to monitor deformations over some key infrastructures of the metropolitan area Barcelona. Several cases of deformation including subsidence and uplift over railways and highway and thermal dilation are shown to prove the capability of the InSAR technique in infrastructure monitoring. In this work, special efforts have been done to improve the density of the points by restructuring the interferograms network and by testing the omega factor.

In conclusion, the InSAR technique is proved to be a powerful tool for precise and continuous monitoring of infrastructure deformations. Early detection of deformation over wide areas is one of the goals of this study. For a better service of infrastructure monitoring, further efforts still need to be focused on increasing the density of the points covering the railways and highways, especially in rural areas, regardless of its orientation while keeping the quality of the selected points.

REFERENCES

Biescas, E., Crosetto, M., Agudo, M., Monserrat, O., Crippa, B., 2007. Two radar interferometric approaches to monitor slow and fast land deformation. Journal of Surveying Engineering, 133(2), 66-71.

Crosetto, M., Monserrat, O., Cuevas-González, M. Devanthéry, N., Crippa, B., 2016. Persistent Scatterer Interferometry: a review. ISPRS Journal of Photogrammetry & Remote Sensing, 115, 78-89

Crosetto, M., Monserrat, O., Cuevas, M. and Crippa, B. 2011. Spaceborne Differential SAR Interferometry: Data Analysis Tools for Deformation Measurement. Remote Sensing, 3, 305-318.

Devanthéry, N., Crosetto, M., Monserrat, O., Cuevas-González, M., Crippa, B. 2014. An approach to Persistent Scatterer Interferometry. Remote Sensing, 6, pp. 6662-6679.

Ferretti, A., Prati, C., Rocca, F., 2000. Nonlinear subsidence rate estimation using permanent scatterers in differential SAR interferometry. IEEE TGARS, 38(5), 2202-2212.

Ferretti, A., Prati, C., Rocca, F., 2001. Permanent scatterers in SAR interferometry. IEEE TGARS, 39(1), 8-20.

Rucci, A., Ferretti, A., Monti Guarnieri, A., Rocca, F. 2012. Sentinel 1 SAR interferometry applications: The outlookfor sub millimeter measurements. Remote Sens. Environ. 120, 156–163

Huang, Q., Crosetto, M., Monserrat, O., Crippa, B. 2017. Displacement monitoring and modelling of a high-speedrailway bridge using C-band Sentinel-1 data. ISPRS J. Photogramm. Remote Sens. 128, 204–211

Tang, P., Chen, F., Guo, H., Tian, B., Wang, X., Ishwaran, N. 2015. Large-area landslides monitoring using advancedmulti-temporal InSAR technique over the giant panda habitat, Sichuan, China. Remote Sens. 7, 8925–8949

Mora, O., Mallorqui, J. J. and Broquetas, A. 2003. Linear and Nonlinear Terrain Deformation Maps From a Reduced Set of Interferometric SAR Images, by IEEE Transactions on Geoscience and Remote Sensing, 41 (10), 2243-2253

Pepe, A., Yang,Y., Manzo, M., Lanari, R. 2015. Improved EMCF-SBAS Processing Chain Based on Advanced Techniques for the Noise-Filtering and Selection of Small Baseline Multi-Look DInSAR Interferograms, IEEE Transactions on Geoscience and Remote Sensing, 53 (8)

Qin, X., Liao, M. Zhang, M. and Yang, M. 2017. Structural Health and Stability Assessment of High-Speed Railways via

Thermal Dilation Mapping With Time-Series InSAR Analysis, IEEE Journal of Selected Topics in Applied Earth Observations and Remote Sensing, vol. 10, no. 6, pp. 2999-3010

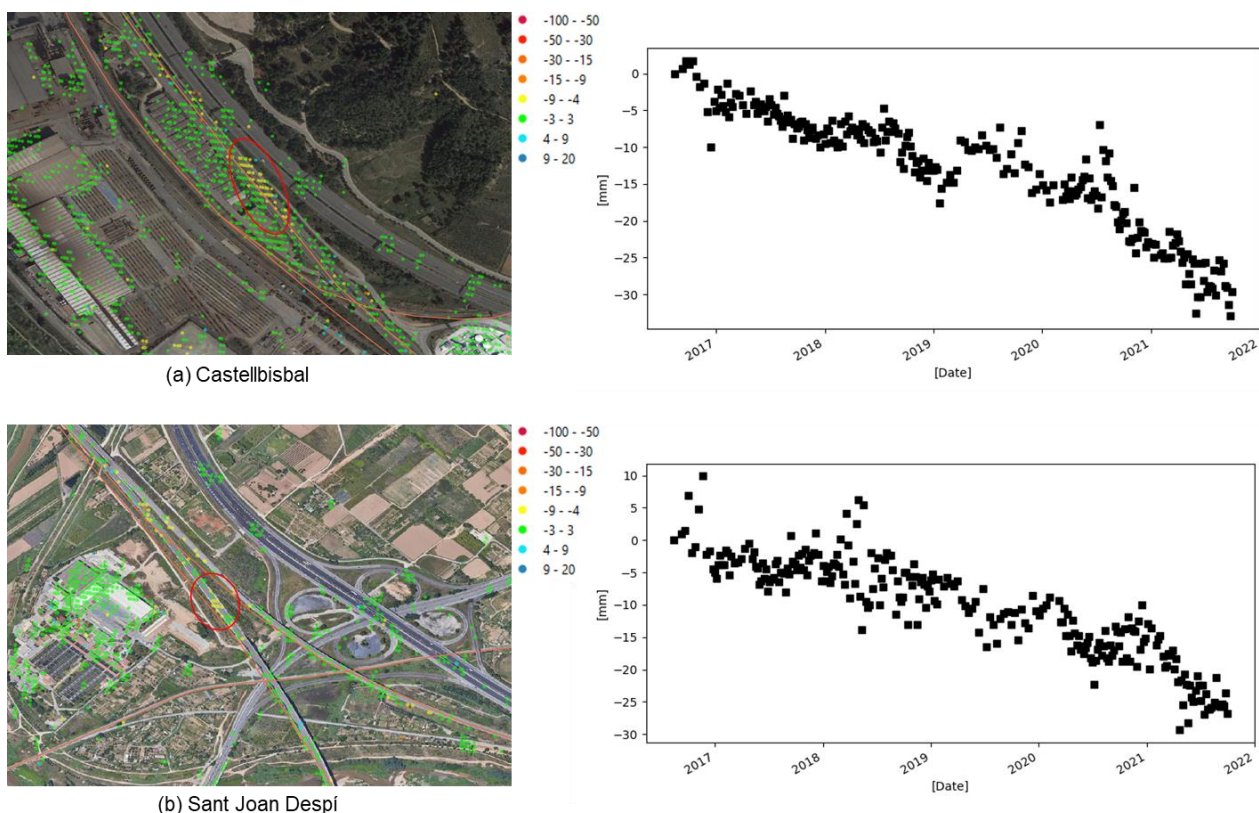## APPENDIX

(a) Castellbisbal

(b) Sant Joan Despí

Figure 8. Examples of subsidence areas with time series on the right. (a) subsidence over railway in Castellbisbal (b) subsidence over highway in Sant Joan Despí
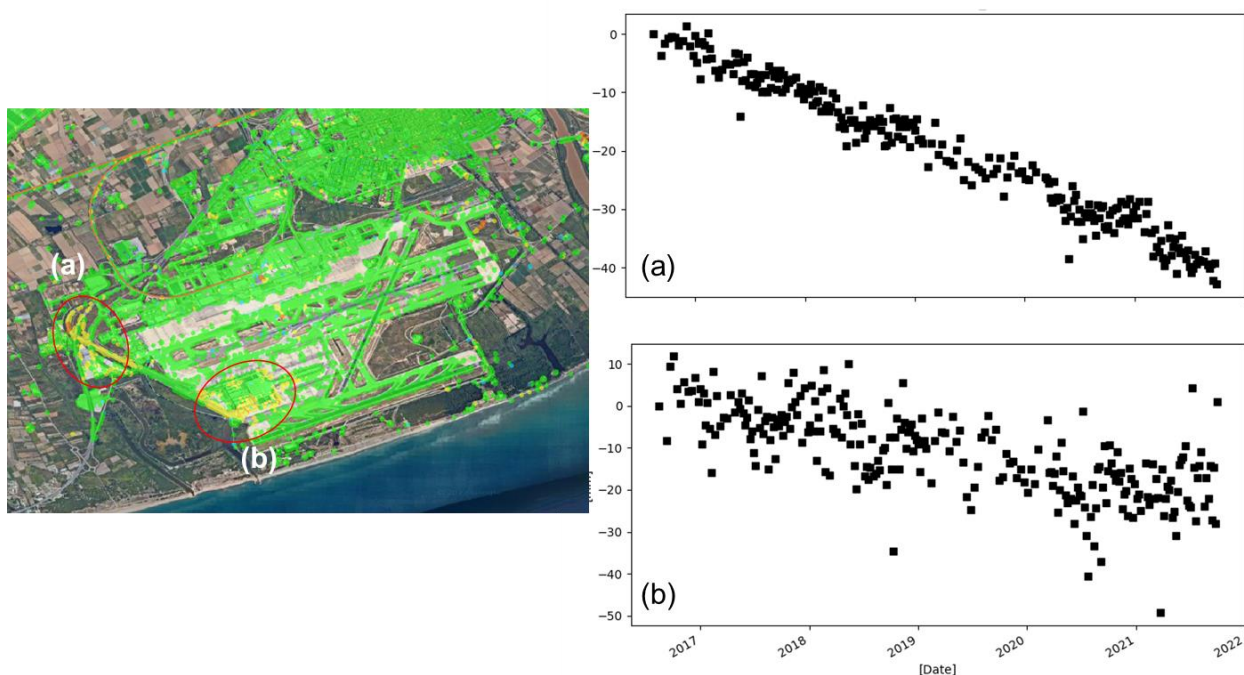

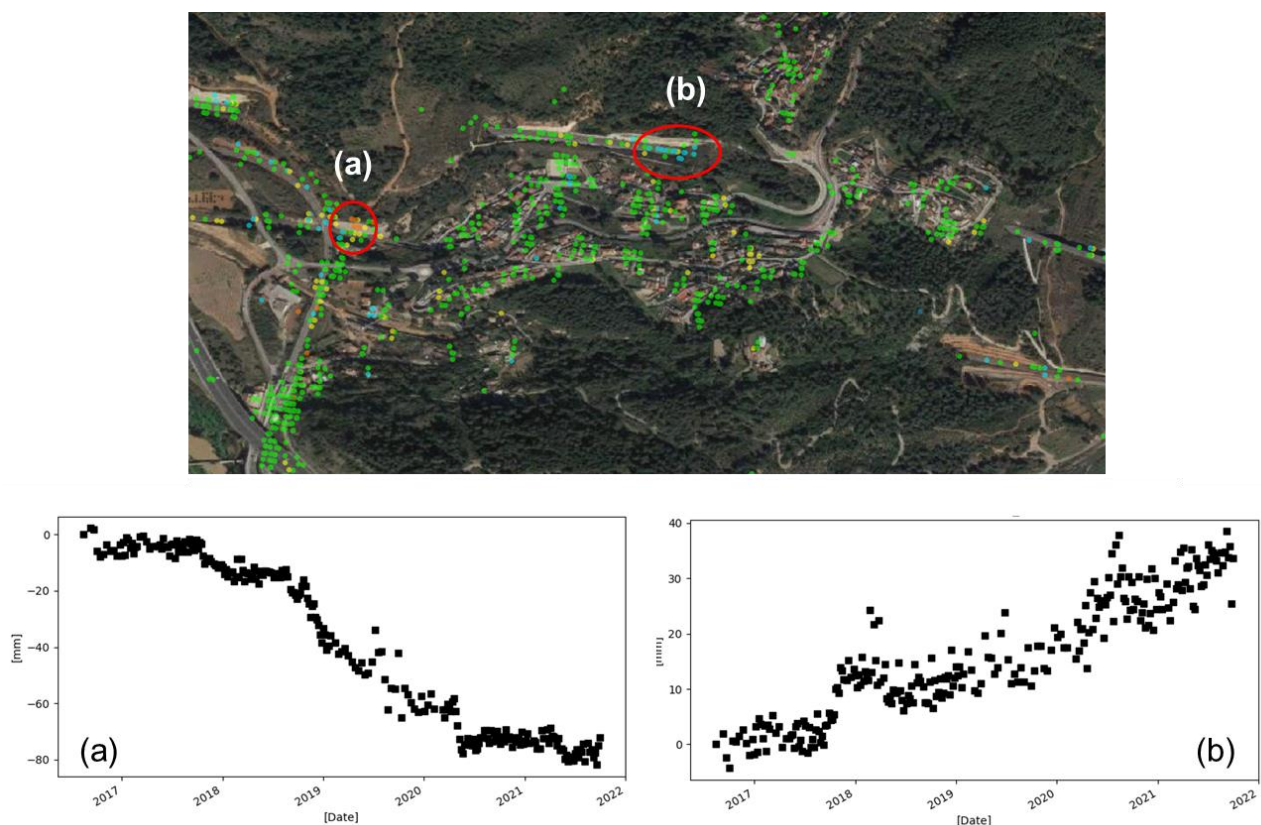**Figure 9.** Subsidence in Aeroport de Barcelona-El Prat

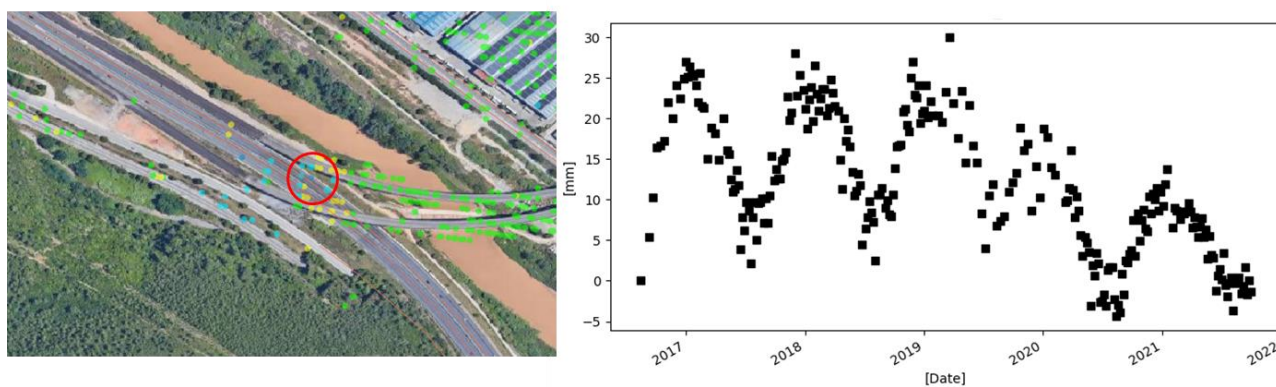**Figure 10.** Subsidence and uplift in mountainous areas where tunnels go through

Figure 11. Examples of thermal dilation